THE JOURNAL OF PHYSICAL CHEMISTRY A
A JOURNAL OF THE AMERICAN CHEMICAL SOCIETY

pubs.acs.org/JPCA Article

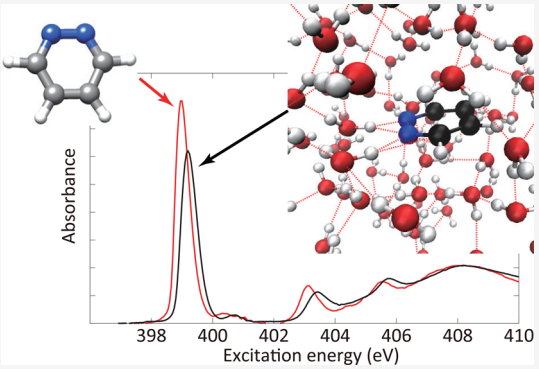
Solvent Effects in the Ultraviolet and X-ray Absorption Spectra of Pyridazine in Aqueous Solution

Shota Tsuru, Bikramjit Sharma, Masanari Nagasaka, and Christof Hättig*

Cite This: J. Phys. Chem. A 2021, 125, 7198–7206 Read Online

ACCESS | Metrics & More | Article Recommendations

ABSTRACT: Electrostatic interaction of the solvent with the solute and fluctuations of the solvent configurations may make excitation energies of the solute different from those in the gas phase. These effects may dominate photoinduced or chemical reaction dynamics in solution systems and can be observed as shifts or broadening of peaks in absorption spectra. In this work, the nitrogen K-edge X-ray absorption spectra were measured for pyridazine in the gas phase and in aqueous solution. The ultraviolet and X-ray absorption spectra of pyridazine in aqueous solution, as well as those in the gas phase, were then calculated with models based on the algebraic−diagrammatic construction through second order [ADC(2)] with the resolution-of-identity (RI) approximation and compared with the spectra obtained in experiments. For aqueous solution, explicit local solvation structures were extracted from an ab initio molecular dynamics (AIMD) trajectory of pyridazine in bulk water, and RI-ADC(2) was combined with the conductor-like screening model (COSMO). The experimental absorption spectra of pyridazine in aqueous solution were reproduced with good accuracy by theoretical treatment of an ensemble containing the explicit local solvation structures of pyridazine with relevant water molecules combined with the COSMO solvation model of water for long-range solvation.



Downloaded via BOCHUM LIBRARIES on August 26, 2021 at 11:50:23 (UTC).
See https://pubs.acs.org/sharingguidelines for options on how to legitimately share published articles.

1. INTRODUCTION

Development of electronic structure theories has enabled quantitative discussion of the pre-edge region in X-ray absorption spectra, which measures core excitations to virtual orbitals.[1,2] Because the excitations to the virtual orbitals are discrete, the pre-edge region sensitively reflects the electronic structure of the initial state. Added to this, main features of X-ray absorption spectroscopy (XAS) such as locality and element selectivity are also advantages for tracking photoinduced or chemical reaction dynamics in pump—probe scheme experiments in the femtosecond time scale. During the past years the wavelength regions of light sources with femtosecond time resolution have been extended. Along with hard X-ray free electron lasers (XFELs), soft XFELs are in user operation at the SPring-8 Å Compact free-electron LAser (SACLA) in Japan,[3] the European XFEL in Hamburg,[4] the Swiss Free electron laser (SwissFEL) at the Paul Scherrer Institut (PSI) in Villigen,[5,6] and the Pohang Accelerator Laboratory X-ray Free-Electron Laser (PAL-XFEL) in South Korea.[7] Meanwhile, femtosecond-to-attosecond time-resolved spectroscopy using high-harmonic generation (HHG) with photon energies in the soft X-ray region have been achieved.[8−11] These time-resolved spectroscopy experiments can also be set in the context of developing compact light sources. Even a new class of ultracompact XFEL sources that can be implemented at the university level is proposed.[12] In this context, tracking photoinduced or chemical reaction dynamics of molecules consisting of light elements with time-resolved (TR) XAS is a new and active research area. Some TR-XAS experiments for small or organic molecules in the gas phase have already been reported.[8−10,13,14]

Because absorption experiments have advantages in investigation into the bulk structure of solutions, application of TR-XAS for tracking photoinduced or chemical reaction dynamics of solution systems is expected. Interactions between solute and solvent may raise or lower the potential energy surfaces, influence the lifetime, or even lead to decay channels different from those in the gas phase. Decay dynamics of thymine excited to the lowest $^1\pi\pi^*$ state is an example of this: On the one hand, in the gas phase, thymine molecules decay after excitation to the lowest $^1n\pi^*$ state with a lifetime of 80 fs and undergo intersystem crossing to the lowest $^3\pi\pi^*$ within ∼3.5 ps.[15] On the other hand, in aqueous solution, the dominant channel is a direct decay to the ground state on a

Received: June 12, 2021
Revised: August 2, 2021
Published: August 11, 2021



© 2021 American Chemical Society

https://doi.org/10.1021/acs.jpca.1c05183
J. Phys. Chem. A 2021, 125, 7198−7206

subpicosecond time scale, and internal conversion to the lowest $^1n\pi^*$ state has not been observed.[16−18] Similar deactivation mechanisms were directly observed for uridine and 5-methyluridine solvated in water with a combination of sub-30 fs transient absorption spectroscopy and quantum dynamics simulations.[19] Hydrogen tunneling dynamics of phenol excited to the lowest $^1\pi\pi^*$ state can be raised as another intriguing example: The O−H bond dissociates by tunneling to the $^1\pi\sigma^*$ state within ∼2.5 ns in the gas phase[20] and ∼5 ns in bulk water.[21] However, at the air−water interface, this reaction proceeds within ∼100 fs.[22]

The understanding of such dynamics in solutions requires spectral calculations together with accurate and efficient sampling of solvation configurations using theoretical tools like molecular dynamics simulations or Monte Carlo methods. To this frontier, density functional based molecular dynamics simulations has become a very popular method not only for sampling configurational space but also for time-dependent properties of systems. The main effects of solute−solvent interactions on electronic excitations are generally of electrostatic origin and related to the solvent polarity. Therefore, dielectric continuum models have been adopted in quantum chemistry, and molecular dynamics simulations have been done based on such quantum chemical methods.[23] Implicit solvent models usually give excitation energies of solution systems with reasonable accuracy. Nonetheless, in some cases, especially when dipole−dipole interactions between the solute and the solvent are locally strong (as e.g. for hydrogen bonds) or change much between the ground and the excited state, the solvatochromic shifts in the UV/vis absorption spectra are not quantitatively reproduced with polarizable continuum models.[24,25] In these cases, further development of computational methods is required to treat the solute and (at least) the closest solvent molecules as a weakly bounded supermolecular system, including the nonperturbative treatment of the effects of local electrostatics and direct solvent−solute interactions. The assessment of the intrinsic accuracy of solvent models for excitation energies is often not straightforward due to difficulty in separating different remaining errors of the solvent model and the electronic structure methods, which can accidentally cancel each other. There can also be other kinds of hindrance specific to the system of interest. In the cases of the photoinduced dynamics of thymine and phenol mentioned above, the prominent excited states, the $^1n\pi^*$ state of thymine and the $^1\pi\sigma^*$ state of phenol, are optically dark, and the experimental values of the excitation energies in aqueous solutions are not available. Even if this is not the case for some molecular species, often the molecules undergo self-association in solution, or their stable conformations are not necessarily the same in the gas phase and in solution. Furthermore, low solubility or close-lying absorption bands of solute and solvent may result in an absorption spectrum of the solute overlapping with the background from the solvent.

In this study, we have undertaken a step toward highly accurate and efficient simulations of molecular dynamics and time-resolved spectra, especially TR-XAS. We have evaluated the valence and core-excitation energies in aqueous solution, calculated with models based on the algebraic−diagrammatic construction through second order with the resolution-of-identity approximation and the conductor-like screening model [COSMO-RI-ADC(2)].[26] ADC(2) is capable of accounting for the dynamical correlation effects of predominantly singly excited state through second order with computational costs scaling with the system size N as $[O(N^5)]$. Because it gives both the XAS spectra[27] and potential energy surfaces[28] with reasonable accuracy, ADC(2) is a natural choice for simulating TR-XAS. The electrostatic solvent effects are taken into account by connection to COSMO,[29] a continuum solvent model which surrounds the solute as a molecular-shaped cavity. Furthermore, to model the solvation more realistically, we have performed an exhaustive ab initio molecular dynamics (AIMD) simulation at finite temperature. Subsequently, a hybrid modeling of solvation comprising the explicit local solvation configurations (from AIMD) and implicit COSMO representation of long-range solvation has been employed.

We chose pyridazine in aqueous solution, for which all the hindrances mentioned above are irrelevant, as the test case. Pyridazine is miscible with water due to hydrogen bonds between the nitrogen lone pairs and the solvent. In contrast to its geometric isomers, self-association is absent from pyridazine dissolved in water.[30] Its three lowest spin-singlet excited states are 1 $^1B_1(n\pi^*)[(8b_2)^1(2a_2)^2]$, 1 $^1A_2(n\pi^*)[(8b_2)^1(3b_1)^2]$, and 2 $^1A_1(\pi\pi^*)[(1a_2)^1(2a_2)^2]$, where the n orbital consists of the nitrogen lone pairs (see Figure 1). The 1 $^1A_2(n\pi^*)$ state is optically dark, and it can be detected only with electron energy loss spectroscopy (EELS).[31] The 1 $^1B_1(n\pi^*)$ and 2 $^1A_1(\pi\pi^*)$ states are detected in UV absorption in both the gas phase[32] and aqueous solution,[30] and solvent effects in the excitation to 1 $^1B_1(n\pi^*)$ are obvious. For investigation into solvent effects in the core excitations, we measured the nitrogen K-edge XAS spectra of pyridazine both in the gas phase and in aqueous solution.

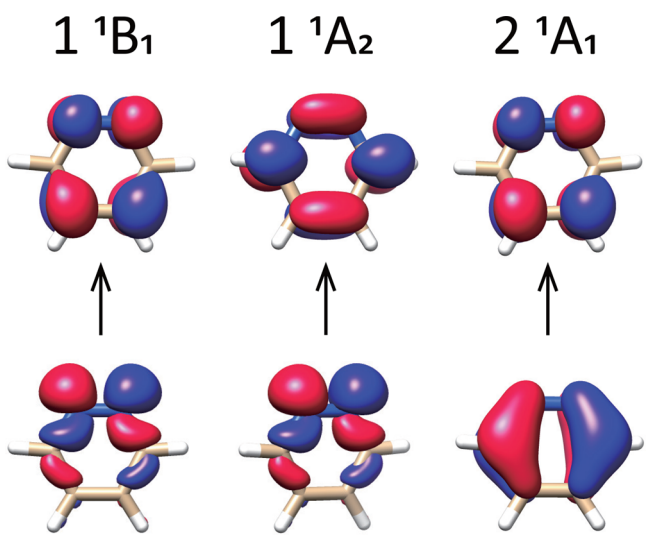


Figure 1. Electronic characteristics of excitations from the ground state to the 1 $^1B_1(n\pi^*)$, 1 $^1A_2(n\pi^*)$, and 2 $^1A_1(\pi\pi^*)$ states of pyridazine.

The paper is organized as follows: First, we describe the AIMD simulation, the models based on COSMO-RI-ADC(2), and the XAS experiment. Next, we compare the calculated valence-excitation energies with the UV absorption spectra. We then compare the N_{1s} core-excitation energies with the XAS spectra in the same manner. In these comparisons, we discuss the dominant factors among the solvent effects and the best model for simulating TR-XAS spectra. Finally, we make a summary assessment of the theoretical models for the spectral analyses.

https://doi.org/10.1021/acs.jpca.1c05183
J. Phys. Chem. A 2021, 125, 7198−7206

2. METHODS

2.1. Molecular Dynamics Simulation for the Generation of Configurations for the Solvation Shell. A representative set of configurations for pyridazine in aqueous solution was generated with an AIMD[33] simulation. To have a reasonable starting geometry of solvated pyridazine in bulk water, we have first performed force-field-based molecular dynamics (ffmd) simulations using Gromacs.[34−37] The force field for the pyridazine molecule was generated by using the ACPYPE[38] tool. We have adopted the TIP4P-2005 water model[39] which is found to be the best rigid, nonpolarizable force field to represent bulk water atomistically.[40] The simulation system contains one pyridazine in 112 water molecules in a cubic box periodically replicated in three dimensions. To fix the box length, we have performed 10 ns long ffmd simulation in the NpT ensemble. The pressure and temperature were kept at 1 atm and 300 K by using Parrinello−Rahman[41] and canonical sampling through velocity rescaling[42] thermostats, respectively. The average box length of 15.0414 Å, found in the NpT simulation was used for the subsequent simulations. Next, starting from a snapshot at the average box length from the NpT trajectory, further a ffmd simulation in the NVT ensemble was performed for 10 ns.

Starting with the final configuration of the ffmd NVT run, we performed an AIMD simulation of the pyridazine in water system using the CP2K package.[43,44] The QUICKSTEP[45] module within CP2K was used to solve the electronic structure which employs a hybrid mode of basis function, that is, a mixture of atom-centered Gaussian functions and plane waves. We have employed the TZV2P Gaussian basis set optimized for the Goedecker−Teter−Hutter pseudopotential.[46−48] The plane wave expansion was truncated at a cutoff of 500 Ry. A revised version of the PBE density functional, namely RPBE,[49] together with Grimme's D3[50] dispersion correction (we refer to this as RPBE-D3 from now onward) was employed in the AIMD simulation. Note that the choice of the RPBE-D3 functional was inspired by its ability to accurately reproduce the underlying many body potential energy surface of liquid water which dictates the accuracy of solvation structures.[51] The AIMD simulation was performed in the NVT ensemble, and the temperature was kept fixed at 300 K (on average) by using massive Nosé−Hoover chain thermostatting[52] with a time constant 167 fs. The equations of motion were integrated by using a time step of 0.5 fs for a total of 106 ps to generate an AIMD trajectory. The first 6 ps of the trajectory was considered as the equilibration phase, and solvation structures from the remaining 100 ps were extracted after every 1 ps for the subsequent quantum chemical calculations of UV and X-ray absorption spectra (*vide infra*). Note that the 6 ps of equilibration was done starting from the already equilibrated ffmd configuration.

2.2. Excitation Energy Calculation and Spectral Simulation. We optimized the ground-state equilibrium or Franck−Condon (FC) geometry using the ORCA package[53,54] at the DFT/RPBE-D3/def2-TZVPP level for consistency with the AIMD simulation. For the gas phase, we calculated the valence and core-excitation energies at the FC geometry, which has C_{2v} symmetry. For the aqueous solution, we calculated those for the four models shown in Figure 2: "FC-COSMO", "Odd-ps set", "Even-ps set", and "Total set". The FC-COSMO model is a pyridazine molecule at the FC geometry surrounded by COSMO. Odd-ps set is an ensemble of 50 snapshots of the AIMD trajectory at 1, 3, 5, ..., 97, 99 ps. Even-ps set is another ensemble of 50 snapshots at 2, 4, 6, ..., 98, 100 ps. Total-set is the combined ensemble of the Odd-ps and Even-ps sets. In each snapshot, water molecules in the first solvation shells of both the pyridazine nitrogen atoms were explicitly taken into account (see section 3.1), whereas the long-range bulk solvation effects were accounted for with COSMO, as shown in Figure 2c. The excitation energies calculated for the Odd-ps and Even-ps models were used to confirm the convergence of the corresponding calculations for the "Total set".

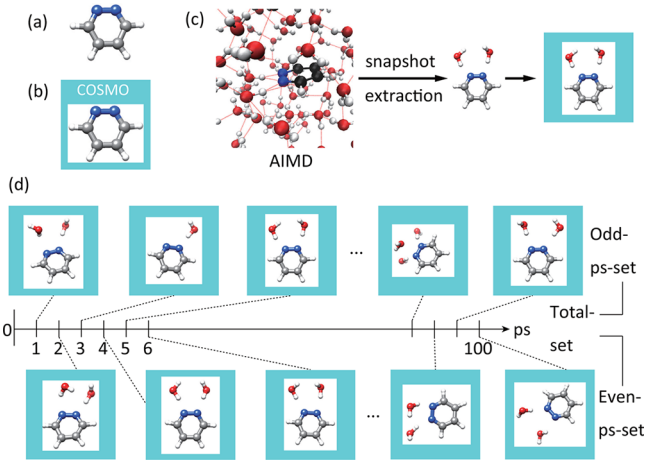


Figure 2. Models to calculate the valence and core-excitation energies: (a) Excitation energies in the gas phase were calculated at the FC geometry optimized at the DFT/RPBE-D3/def2-TZVPP level. (b) "FC−COSMO model" for the aqueous solution. The solvent was accounted for with COSMO, and the excitation energies were calculated at the FC geometry. (c) Modeling scheme for a snapshot extracted from the AIMD trajectory. The water molecules in the first solvation shell of both the pyridazine nitrogen atoms were explicitly taken into account, whereas the long-range solvation was expressed with COSMO. (d) The "Odd-ps set" consists of the snapshots of the AIMD trajectory at 1, 3, 5, ..., 99 ps. The "Even-ps set" consists of the snapshots at 2, 4, 6, ..., 100 ps. The "Total set" is the combined ensemble of the Odd-ps set and Even-ps set.

We calculated the valence and core-excitation energies at the RI-ADC(2)/aug-cc-pVTZ level for all the models, with the TURBOMOLE V7.5 electronic structure package.[55,56] Where not otherwise stated, we used for the calculations with the COSMO solvation model the post self-consistent field (SCF) reaction field scheme as described in refs 26 and 57. To clarify the dominant factor of the solvent effects, we performed additional calculations for the excitation energies within the frozen solvent approximation[58] for the FC-COSMO model: We optimized the molecular orbitals with COSMO-Hartree−Fock. The RI-ADC(2) calculations were then carried for the COSMO-Hartree−Fock reference without including the additional linear response coupling terms of the post-SCF reaction field scheme. For the core excitations we employed the core−valence separation (CVS) approximation[59] for the RI-ADC(2) calculations as described in ref 60.

For comparison with the X-ray absorption experiments, we convoluted the oscillator strengths with a Lorentzian function (FWHM = 0.52 eV, which was determined from the gas-phase XAS spectrum). To construct the XAS spectrum of the aqueous solution, we convoluted the oscillator strengths for each snapshot of the Total-set in the above-mentioned way and averaged the snapshot spectra.

https://doi.org/10.1021/acs.jpca.1c05183
J. Phys. Chem. A 2021, 125, 7198−7206

2.3. XAS Experiment. The XAS experiment was performed at the soft X-ray undulator beamline BL3U at the UVSOR-III Synchrotron.[61] A detailed description of the liquid cell for XAS in transmission mode is available elsewhere.[62,63] The liquid cell was in an ambient pressure of helium gas, where a liquid layer was sandwiched between two SiC membranes with a thickness of 100 nm. Liquid samples were exchanged by using a tubing pump without changing the position of the liquid cell. The liquid temperature was set to 25 °C by using a chiller system. The ambient helium chamber was separated by a small SiC window (0.2×0.2 mm^2) from the beamline under ultrahigh-vacuum conditions. In the nitrogen K-edge XAS spectrum of 0.5 M pyridazine aqueous solution, the absorbance A was defined as $A = \ln(I_0/I)$, where I_0 and I are the transmission signals of neat water and pyridazine solutions, respectively. The intensities of transmitted soft X-rays were counted by a photodiode detector. For getting appropriate absorbance of soft X-rays, the liquid thickness was controlled by adjusting the helium pressure around the liquid cell.[64] The nitrogen K-edge gas-phase XAS spectrum was measured for pyridazine evaporated from liquid by bubbling with helium gas. Note that the absorbance of the gas-phase spectrum was optimized by controlling the mixing ratio of pyridazine vapor and helium gas with two mass flow controllers. The energy resolution was set to 0.2 eV. The photon energy was calibrated by the peak of the polymer film,[64] which was related to the N 1s → π^* band of nitrogen gas.[65]

3. RESULTS AND DISCUSSION

3.1. Selection of Solvation Configurations. Figure 3 shows the radial distribution functions (RDFs) of the (blue) hydrogen and (red) oxygen atoms of the solvent water molecules around the pyridazine nitrogen atoms obtained from the AIMD simulation. The first peak of the hydrogen radial distribution function starts to grow around 1.4 Å and has its maximum at 1.8 Å. Thereafter, the RDF reaches a minimum at 2.3 Å. The first peak of the oxygen RDF starts to grow around 2.5 Å and has its maximum at 2.8 Å. The minimum of this RDF at 3.08 Å demarcates the first solvation shell around the pyridazine nitrogen atoms. For the models with explicit solvent (Figure 2c) we have considered all the water molecules in the first solvation shell of both the pyridazine nitrogen atoms to explicitly account for the short-range solvation effects on the UV and X-ray absorption spectra in subsequent sections. Figure 4 shows the distribution of the number of water molecules in the first solvation shell with respect to the nitrogen atoms. The largest probability is observed for two followed by significant probabilities of one and three water molecules. Note that these are the distributions of water molecules in the first solvation shell of both the pyridazine nitrogen atoms. This should not be confused with the distribution in the first solvation shell with respect to the pyridazine nitrogen atoms which requires normalization by a factor of 2 (number of pyridazine nitrogen atoms).

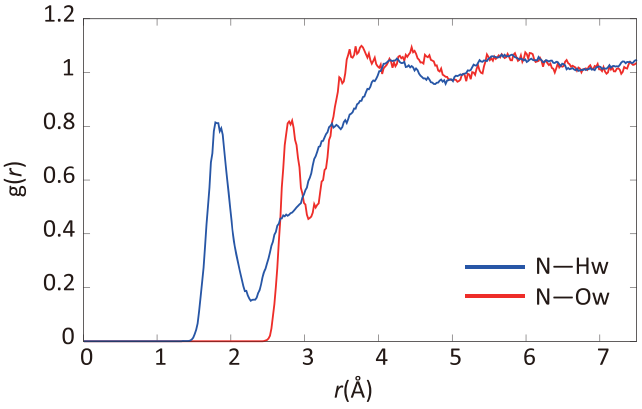


Figure 3. Radial distribution functions of (blue) hydrogen and (red) oxygen atoms of the solvent water molecules with respect to the pyridazine nitrogen atoms. The cutoffs of the first peaks of hydrogen and oxygen atoms are 2.3 and 3.08 Å, respectively.

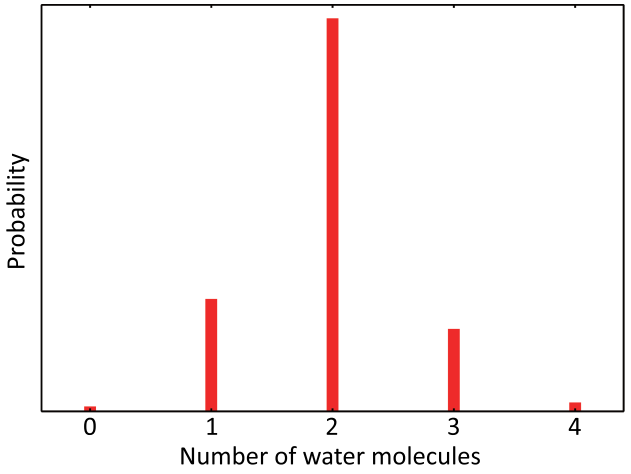


Figure 4. Distribution of the number of water molecules in the first solvation shell of both the pyridazine nitrogen atoms.

3.2. UV Absorption. Table 1 shows the excitation energies of the three lowest excited states calculated for the gas phase and the four models for the aqueous solution. In Table 1, the excitations energies obtained in the UV absorption,[30,32] and EELS[31] experiments are also listed. We also show the excitation energies of the 2 $^1A_2(n\pi^*)$ and 2 $^1B_1(n\pi^*)$ states in the gas phase, obtained from the calculation and the EELS experiment, to evaluate the accuracy of the present calculations. The excitation energies of the dipole-allowed states from UV absorption spectroscopy and EELS agree

Table 1. Valence-Excitation Energies (eV) and Comparison with Experimental Values from UV Absorption Spectroscopy (Gas),[32] EELS,[31] and UV Absorption Spectroscopy (Aqueous Solution)[30]

	gas	FC-COSMO	snapshot ensemble	UV abs	EELS
1 $^1B_1(n\pi^*)$	3.77	4.10	4.17 (Odd-ps)	3.58 (gas)	3.63
			4.21 (Even-ps)	4.16 (aq)	
			4.19 (Total)		
1 $^1A_2(n\pi^*)$	4.24	4.65	4.77 (Odd-ps)		4.02
			4.74 (Even-ps)		
			4.75 (Total)		
2 $^1A_1(\pi\pi^*)$	5.28	5.34	5.36 (Odd-ps)	5.10 (gas)	5.01
			5.37 (Even-ps)	5.00 (aq)	
			5.37 (Total)		
2 $^1A_2(n\pi^*)$	5.72				5.61
2 $^1B_1(n\pi^*)$	6.26				6.00

https://doi.org/10.1021/acs.jpca.1c05183
J. Phys. Chem. A 2021, 125, 7198−7206

within 0.1 eV. The calculated energy differences between the five excited states match those from EELS with errors within ≈0.2 eV, which corresponds to the accuracy expected from ADC(2) for valence transitions in closed-shell molecules dominated by single excitations. Therefore, the excitation energies calculated at the (COSMO-)RI-ADC(2)/aug-cc-pVTZ level are reasonably accurate for discussing the solvent effects in the UV absorption. Differences within 0.05 eV between the Odd-ps and Even-ps results indicate sufficient convergence of the results with respect to the number of snapshots. Our discussion below is based on the excitation energies calculated for Total-set, which is the combined ensemble of Odd-ps and Even-ps (see Figure 2).

Figure 5 shows the UV absorption spectra digitized from ref 32 (gas, red curve) and ref 30 (aqueous solution, blue curve),

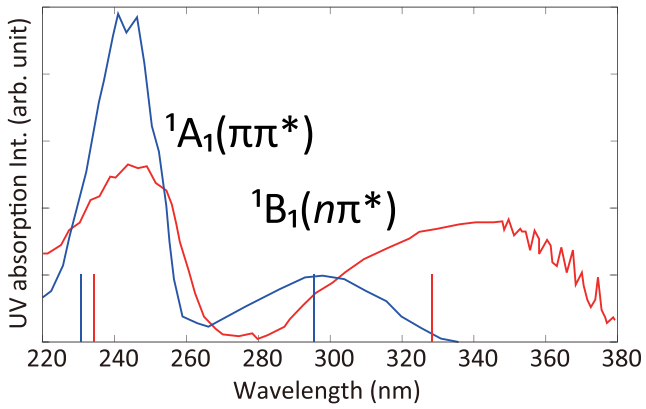


Figure 5. UV absorption spectra of pyridazine in the (red) gas phase and (blue) aqueous solution, which were adapted with permission from ref 32 (Copyright 2020 Elsevier) and ref 30 (Copyright 2003 Elsevier), respectively. Bars indicate the excitation energies of 1 $^1B_1(n\pi^*)$ and 2 $^1A_1(\pi\pi^*)$ calculated for (red) the gas phase and (blue) Total-set.

along with excitation energies of 1 $^1B_1(n\pi^*)$ and 2 $^1A^1(\pi\pi^*)$ calculated for (red) the gas phase and (blue) Total-set. The excitation energy of the first $^1B_1(n\pi^*)$ state in the UV absorption spectra in aqueous solution is 0.58 eV higher than that in the gas phase. The major part of this difference has been reproduced by the FC-COSMO calculation: The excitation energy calculated with FC-COSMO is 0.33 eV higher than that calculated for the gas phase. The excitation energy is further 0.09 eV higher for Total-set, where the first solvation shell was explicitly taken into account. We do not expect a further improvement of the accuracy by taking the second solvation shell into account because of the limitations of the electronic structure methods used for the excitation energies and the AIMD simulation. The 1 $^1B_1(n\pi^*)$ excitation energy obtained with the frozen solvent approximation is 0.35 eV higher than that in the gas phase, and this energy difference is almost the same as the normal FC-COSMO result. As explained in section 2.2, the frozen solvent approximation neglects the response of the reaction field to the excitation process and only accounts for the static charge distribution of the reaction field equilibrated with the Hartree−Fock ground state. Therefore, this result indicates that the dominant factor of the solvent effect on the 1 $^1B_1(n\pi^*)$ excitation energy of pyridazine is the stabilization of the nitrogen lone pairs by hydrogen bonds with the solvent water molecules. We can thus conclude that the major part of the solvent effect can be described by the FC-COSMO model. The solvent effect can be more quantitatively described by an ensemble of snapshots, where the first solvent water molecules are explicitly taken into account, from the AIMD trajectory.

Because it also originates from the nitrogen lone pairs, the first $^1A_2(n\pi^*)$ excitation energies calculated for the gas phase, FC-COSMO, and Total-set exhibit a similar solvent effect. In contrast to these two $n\pi^*$ states, the overall solvent shift for the 2 $^1A^1(\pi\pi^*)$ absorption band is much smaller. This is also the case in the calculations: The calculated 2 $^1A_1(\pi\pi^*)$ excitation energy is 5.28, 5.37, 5.34, and 5.37 eV for the gas phase, frozen solvent approximation, FC-COSMO, and Total-set, respectively.

3.3. X-ray Absorption. Figure 6 shows the nitrogen K-edge XAS spectra of pyridazine in the gas phase and aqueous

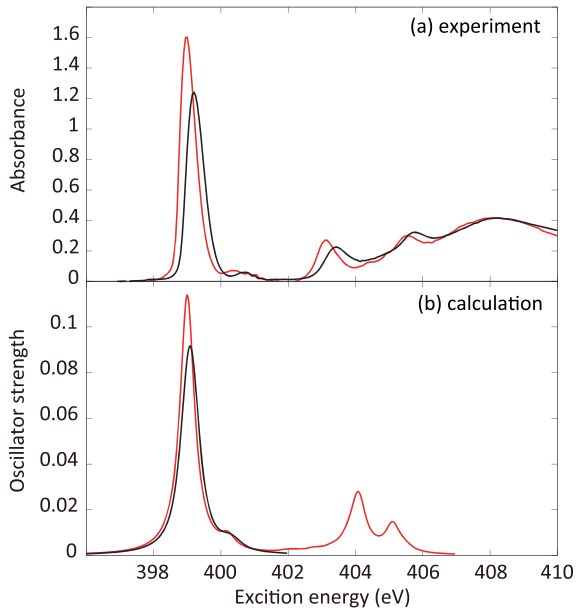


Figure 6. Nitrogen K-edge XAS spectra of pyridazine in the (red) gas phase and (black) aqueous solution, obtained in the (a) experiments and (b) calculations. The calculated spectra have for better comparability been shifted by −3.03 eV. Note that the calculated spectra have only been evaluated up to ≈406 and ≈402 eV for the gas phase and aqueous solution, respectively.

solution, obtained from the experiments and the calculations. We normalized the experimental results for the gas phase and the aqueous solution to the same value of area and shifted the calculated spectra by −3.03 eV to match the main peak in the gas-phase spectra. We also shifted the calculated core-excitation energies in the tables and text by −3.03 eV throughout. We calculated the XAS spectra of the aqueous solution with the Total-set model. The natural transition orbitals (NTOs)[66−69] of the N_{1s} core excitations from the ground state at the FC geometry in the gas phase are given in Table 2. In the gas phase, the main peak is at 399 eV. This peak is assigned to the $1b_2 \rightarrow 2a_2$ ($1B_1$) transition, where the $1b_2$ orbital is the delocalized ungerade N_{1s} orbital. The $1a_1 \rightarrow 2a_2$ ($1A_2$) transition, where the $1a_1$ orbital is the delocalized gerade N_{1s} orbital, is dipole-forbidden. This peak can be interpreted as a combination of two peaks for the transitions from the localized N_{1s} orbitals to the $2a_2$ virtual orbital. The second peak appears at 400.3 eV in the experiment and 400.19 eV in the calculation in the gas phase. This peak is assigned to

https://doi.org/10.1021/acs.jpca.1c05183
J. Phys. Chem. A 2021, 125, 7198−7206

Table 2. Energies, Strengths, and NTOs of the N_{1S} Core Excitations from the Ground State at the FC Geometry in the Gas Phase (NTO Isosurface Is 0.05)

Final state	Ex. energy (eV)	Osc. strength	Hole	Particle
$1B_1$	399.00	0.0927		
$1A_2$	399.01	-		
$2A_2$	400.19	-		
$2B_1$	400.21	0.0044		
$6B_1$	404.09	0.0184		
$6A_2$	404.11	-		
$7B_1$	405.11	0.0099		
$7A_2$	405.13	-		

the $2A_2$ and $2B_1$ transitions to the $3b_1$ orbital. The intensity of the second peak is only 5% of the first peak because the $3b_1$-orbital density is distributed over all the nitrogen and carbon atoms and delocalized over the N═N bond. The small vibrational structure around 401 eV in the gas-phase XAS spectra originates from background of remaining nitrogen gas. The peaks at 403.1 and 404.5 eV in the experiment for the gas phase, which appear at 404.09 and 405.11 eV in the calculation, respectively, originate from transitions dominated by $N_{1s} \rightarrow 3a^2$ (former is $6B_1$ and $6A_2$, latter is $7B_1$ and $7A_2$). We do not discuss the higher-energy region, where a different theoretical scheme would be required. It should also be noted that there are more than 30 roots lying below the $6B_1$ state, including dipole-forbidden states. Such a larger number of roots hinders convergence in the calculations without the C_{2v} symmetry and quantitative discussion of the respective target states in solution. Therefore, we focus on the first four N_{1s} excitations to discuss solvent effects.

In the experiment, the XAS spectrum of pyridazine aqueous solution exhibits the first and second peaks at 399.2 and 400.7 eV, respectively. They are blue-shifted by 0.2 and 0.4 eV with respect to the gas-phase spectrum. In addition, the FWHM of the main peak is 0.52 and 0.65 eV for the gas phase and the aqueous solution, respectively, and the height in the spectrum of the aqueous solution is only 77% of that in the gas-phase spectrum. This is interpreted as peak broadening due to fluctuation of the solvation environment. Table 3 shows the four lowest core-excitation energies calculated for the gas phase, FC-COSMO, and Total-set. For the Total-set calculations, the shifts from the gas-phase results and the standard deviations are also given. In the FC-COSMO calculations, the $1B_1$, $1A_2$, $2A_2$, and $2B_1$ excitation energies are blue-shifted by 0.09, 0.09, 0.14, and 0.14 eV with respect to the gas-phase results, respectively. These shifts are almost the same in the frozen solvent calculations. Therefore, the blue-

Table 3. Four Lowest N_{1s} Core-Excitation Energies (eV) Calculated for the Gas Phase, FC-COSMO, and Snapshot Ensemble (Total-Set); Shifts of Energies from Those in the Gas Phase and Standard Deviations in the Calculations for Total-Set Are Also Shown

	gas	FC-COSMO	snapshot ensemble	shift	std dev
$1B_1$	399.00	399.09	399.04	0.04	0.13
$1A_2$	399.01	399.10	399.17	0.16	0.27
$2A_2$	400.19	400.33	400.28	0.09	0.29
$2B_1$	400.21	400.35	400.41	0.20	0.33

shifts can be attributed to the interaction of the change of the charge density upon excitation with the electrostatic potential of the solvent as equilibrated with the ground state of pyridazine. In the Total-set calculations, where water molecules in the first solvation shell were explicitly taken into account, the blue-shifts are not necessarily larger than those in the FC-COSMO calculations, while the standard deviations are always larger than the shifts. These standard deviations around the mean value of the excitation energies for the snapshots in this set are attributed to fluctuation of the water molecules that have hydrogen bonds with the pyridazine nitrogen atoms. It should also be noted that the C_{2v} symmetry of pyridazine is broken in the individual snaphots of the Total-set calculations and, therefore the oscillator strengths of the first and second transitions ($1B_1$ and $1A_2$) are similar for the snapshots. This is also the case for the third and fourth transitions. In the calculated XAS spectrum of the aqueous solution, the first and second peaks appear at 399.08 and ~400.2 eV, respectively. The values for the blue-shift of the first peak are 0.2 and 0.08 eV in the experiment and the calculation, respectively. The value for the blue-shift of the second peak in the calculation is <0.1 eV, which is somewhat smaller than the blue-shift of 0.4 eV in the experiment. The FWHM of the main peak in the XAS spectrum computed with the Total-set model is 0.65 eV, which is exactly the same as that in the experiment, and the height of the main peak in the XAS spectrum averaged over the snapshots is 81% of that in the gas-phase spectrum. Although the values for the blue-shifts of the peaks in the calculation are smaller than those in the experiment, the broadening of the peaks quantitatively agrees between the experiment and calculation. Therefore, one can say that the geometrical fluctuation effect in the aqueous solution XAS spectrum is well reproduced by extracting snapshots from the AIMD trajectory and explicitly taking water molecules in the first solvation shell of the pyridazine nitrogen atoms into account.

3.4. Assessment of Modeling Solvation with COSMO.

As we have shown, the Total-set model quantitatively reproduces the solvent effects both in the UV and X-ray absorption spectra. However, a calculation based on the Total-set model, which comprises an AIMD simulation and iterative calculations of the excitation energies for the AIMD snapshots, is time-consuming compared to the single calculation based on the FC-COSMO model, where all the solvent is modeled with COSMO. Aiming at efficient analyses of the UV/vis and X-ray absorption spectra, we discuss the FC-COSMO model's capability of reproducing the solvent effects in the absorption spectra.

The solvent effects in the absorption spectra have five aspects: (i) electrostatic interaction between solute and solvent in the initial state, (ii) excitonic coupling of the transition

https://doi.org/10.1021/acs.jpca.1c05183
J. Phys. Chem. A 2021, 125, 7198−7206

density to the solvent polarizability, (iii) the electrostatic interaction in the excited state, (iv) fluctuation of the solute's geometry, and (v) solvent fluctuations, although the last two aspects are often difficult to disentangle. In the UV/vis absorption, FC-COSMO with the post-SCF reaction field scheme as used in this work reproduces the solvatochromic shifts due to the effects i and ii within an error of ≈0.1 eV compared to the Total-set model even in the case where the solute has hydrogen bonds with the solvent molecules. Effect v is negligible compared to the electrostatic effect and the vibrational broadening in the UV/vis absorption, and implicitly included in the solvent models. Therefore, if the solute molecule is rigid, FC-COSMO often works well for a qualitative analysis of an UV/vis absorption spectrum.

It should however be noted that FC-COSMO cannot take energy dissipation from a solute to the solvent during photoinduced dynamics into account. For such dynamics simulations, at least the closest solvent molecules need to be explicitly included in the supermolecular system.

When it comes to quantitative discussion on the solvent effects in the X-ray absorption, FC-COSMO does not work well because effect v is large compared to the small lifetime and vibrational broadenings, while effects i and ii are small. Nevertheless, as we have found in the present measurements, such a broadening effect due to the solvent in the XAS spectra is not so large that it affects assignment of the peaks. Therefore, FC-COSMO sufficiently works for the assignments. It is worth emphasizing that since the peaks are narrow, effect iv on a XAS spectrum could be employed to investigate the solute's geometry. Once this performance has been confirmed, FC-COSMO may work even for qualitative analysis of the TR-XAS spectra.

4. CONCLUSION

We measured the nitrogen K-edge X-ray absorption spectra of pyridazine in the gas phase and in aqueous solution. We then investigated the solvent effects on the UV and X-ray absorption spectra of pyridazine aqueous solution with a combination of an AIMD simulation and COSMO-RI-ADC(2) calculations. We attributed the blue-shifts of the nπ^* excitations, where the n orbital consists of the nitrogen lone pairs, to stabilization of the n orbital by hydrogen bonds with the solvent water molecules. We then attributed the peak shift and broadening observed in the XAS spectrum of the aqueous solution to fluctuations of the solvent water molecules. We reproduced both effects by calculations for an ensemble of solvent configurations extracted from the AIMD trajectory, expressing the solvent except for the first solvation shell with COSMO.

AUTHOR INFORMATION

Corresponding Author

Christof Hättig − *Lehrstuhl für Theoretische Chemie, Ruhr-Universität Bochum, D-44780 Bochum, Germany;* orcid.org/0000-0002-5752-2710; Phone: +49 (0)234 32 28082; Email: Christof.Haettig@ruhr-uni-bochum.de

Authors

Shota Tsuru − *Lehrstuhl für Theoretische Chemie, Ruhr-Universität Bochum, D-44780 Bochum, Germany;* orcid.org/0000-0003-0014-7873

Bikramjit Sharma − *Lehrstuhl für Theoretische Chemie, Ruhr-Universität Bochum, D-44780 Bochum, Germany;* orcid.org/0000-0002-8844-1796

Masanari Nagasaka − *Institute for Molecular Science and SOKENDAI (The Graduate University for Advanced Studies), Okazaki 444-8585, Japan;* orcid.org/0000-0002-6249-6553

Complete contact information is available at: https://pubs.acs.org/10.1021/acs.jpca.1c05183

Notes

The authors declare no competing financial interest.

ACKNOWLEDGMENTS

We acknowledge Prof. D. Marx, Lehrstuhl für Theoretische Chemie, Ruhr-Universität Bochum, Germany, for his support. This research was funded by the Alexander von Humboldt Foundation through a Research Fellowship to S.T. (JPN 1201668 HFST-P) and the Deutsche Forschungsgemeinschaft (DFG, German Research Foundation) under Germany's Excellence Strategy EXC 2033-390677874-RESOLV. We are grateful to the staff members of the UVSOR-III Synchrotron for their kind support.

REFERENCES

(1) Norman, P.; Dreuw, A. Simulating X-ray Spectroscopies and Calculating Core-Excited States of Molecules. *Chem. Rev.* **2018**, *118*, 7208−7248.

(2) Tsuru, S.; Vidal, M. L.; Pápai, M.; Krylov, A. I.; Møller, K. B.; Coriani, S. An assessment of different electronic structure approaches for modeling time-resolved x-ray absorption spectroscopy. *Struct. Dyn.* **2021**, *8*, 024101.

(3) Owada, S.; Togawa, K.; Inagaki, T.; Hara, T.; Tanaka, T.; Joti, Y.; Koyama, T.; Nakajima, K.; Ohashi, H.; Senba, Y.; et al. A soft X-ray free-electron laser beamline at SACLA: the light source, photon beamline and experimental station. *J. Synchrotron Radiat.* **2018**, *25*, 282−288.

(4) Tschentscher, T.; Bressler, C.; Grünert, J.; Madsen, A.; Mancuso, A. P.; Meyer, M.; Scherz, A.; Sinn, H.; Zastrau, U. Photon Beam Transport and Scientific Instruments at the European XFEL. *Appl. Sci.* **2017**, *7*, 592.

(5) Milne, C. J.; Schietinger, T.; Aiba, M.; Alarcon, A.; Alex, J.; Anghel, A.; Arsov, V.; Beard, C.; Beaud, P.; Bettoni, S.; et al. SwissFEL: The Swiss X-ray Free Electron Laser. *Appl. Sci.* **2017**, *7*, 720.

(6) Prat, E.; Abela, R.; Aiba, M.; Alarcon, A.; Alex, J.; Arbelo, Y.; Arrell, C.; Arsov, V.; Bacellar, C.; Beard, C.; et al. A compact and cost-effective hard X-ray free-electron laser driven by a high-brightness and low-energy electron beam. *Nat. Photonics* **2020**, *14*, 748−754.

(7) Ko, I. S.; Kang, H.-S.; Heo, H.; Kim, C.; Kim, G.; Min, C.-K.; Yang, H.; Baek, S. Y.; Choi, H.-J.; Mun, G.; et al. Construction and Commissioning of PAL-XFEL Facility. *Appl. Sci.* **2017**, *7*, 479.

(8) Bhattacherjee, A.; Pemmaraju, C. D.; Schnorr, K.; Attar, A. R.; Leone, S. R. Ultrafast Intersystem Crossing in Acetylacetone via Femtosecond X-ray Transient Absorption at the Carbon K-Edge. *J. Am. Chem. Soc.* **2017**, *139*, 16576−16583.

(9) Attar, A. R.; Bhattacherjee, A.; Pemmaraju, C. D.; Schnorr, K.; Closser, K. D.; Prendergast, D.; Leone, S. R. Femtosecond x-ray spectroscopy of an electrocyclic ring-opening reaction. *Science* **2017**, *356*, 54−59.

(10) Saito, N.; Sannohe, H.; Ishii, N.; Kanai, T.; Kosugi, N.; Wu, Y.; Chew, A.; Han, S.; Chang, Z.; Itatani, J. Real-time observation of electronic, vibrational, and rotational dynamics in nitric oxide with attosecond soft x-ray pulses at 400 eV. *Optica* **2019**, *6*, 1542−1546.

(11) Barreau, L.; Ross, A. D.; Garg, S.; Kraus, P. M.; Neumark, D. M.; Leone, S. R. Efficient table-top dual-wavelength beamline for ultrafast transient absorption spectroscopy in the soft X-ray region. *Sci. Rep.* **2020**, *10*, 5773.

(12) Rosenzweig, J. B.; Majernik, N.; Robles, R. R.; Andonian, G.; Camacho, O.; Fukasawa, A.; Kogar, A.; Lawler, G.; Miao, J.; Musumeci, P.; et al. An ultra-compact x-ray free-electron laser. *New J. Phys.* **2020**, *22*, 093067.
(13) Wolf, T. J. A.; Myhre, R. H.; Cryan, J. P.; Coriani, S.; Squibb, R. J.; Battistoni, A.; Berrah, N.; Bostedt, C.; Bucksbaum, P.; Coslovich, G.; et al. Probing ultrafast $\pi\pi^*/n\pi^*$ internal conversion in organic chromophores via K-edge resonant absorption. *Nat. Commun.* **2017**, *8*, 29.
(14) Scutelnic, V.; Tsuru, S.; Pápai, M.; Yang, Z.; Epshtein, M.; Xue, T.; Haugen, E.; Kobayashi, Y.; Krylov, A. I.; Møller, K. B. et al. X-ray transient absorption reveals the $^1A_u(n\pi^*)$ state of pyrazine in electronic relaxation. *Nat. Commun.* **2021**, to be published.
(15) Wolf, T. J. A.; Parrish, R. M.; Myhre, R. H.; Martínez, T. J.; Koch, H.; Gühr, M. Observation of Ultrafast Intersystem Crossing in Thymine by Extreme Ultraviolet Time-Resolved Photoelectron Spectroscopy. *J. Phys. Chem. A* **2019**, *123*, 6897−6903.
(16) Buchner, F.; Nakayama, A.; Yamazaki, S.; Ritze, H.-H.; Lübcke, A. Excited-State Relaxation of Hydrated Thymine and Thymidine Measured by Liquid-Jet Photoelectron Spectroscopy: Experiment and Simulation. *J. Am. Chem. Soc.* **2015**, *137*, 2931−2938.
(17) Pilles, B. M.; Maerz, B.; Chen, J.; Bucher, D. B.; Gilch, P.; Kohler, B.; Zinth, W.; Fingerhut, B. P.; Schreier, W. J. Decay Pathways of Thymine Revisited. *J. Phys. Chem. A* **2018**, *122*, 4819−4828.
(18) Erickson, B. A.; Heim, Z. N.; Pieri, E.; Liu, E.; Martinez, T. J.; Neumark, D. M. Relaxation Dynamics of Hydrated Thymine, Thymidine, and Thymidine Monophosphate Probed by Liquid Jet Time-Resolved Photoelectron Spectroscopy. *J. Phys. Chem. A* **2019**, *123*, 10676−10684.
(19) Cerullo, G.; Borrego-Varillas, R.; Nenov, A.; Kabacinski, P.; Conti, I.; Ganzer, L.; Oriana, A.; Delfino, I.; Weingart, O.; Manzoni, C.; et al. Tracking excited state decay mechanisms of pyrimidine nucleosides in real time. Research Square, 2020; DOI: 10.21203/rs.3.rs-97259/v1, under review in *Nat. Chem.*
(20) Roberts, G. M.; Chatterley, A. S.; Young, J. D.; Stavros, V. G. Direct Observation of Hydrogen Tunneling Dynamics in Photoexcited Phenol. *J. Phys. Chem. Lett.* **2012**, *3*, 348−352.
(21) Oliver, T. A. A.; Zhang, Y.; Roy, A.; Ashfold, M. N. R.; Bradforth, S. E. Exploring Autoionization and Photoinduced Proton-Coupled Electron Transfer Pathways of Phenol in Aqueous Solution. *J. Phys. Chem. Lett.* **2015**, *6*, 4159−4164.
(22) Kusaka, R.; Nihonyanagi, S.; Tahara, T. The photochemical reaction of phenol becomes ultrafast at the air-water interface. *Nat. Chem.* **2021**, *13*, 306−311.
(23) Herbert, J. M. Dielectric continuum methods for quantum chemistry. *Wiley Interdiscip. Rev.: Comput. Mol. Sci.* **2021**, *11*, e1519.
(24) Rondi, A.; Rodriguez, Y.; Feurer, T.; Cannizzo, A. Solvation-Driven Charge Transfer and Localization in Metal Complexes. *Acc. Chem. Res.* **2015**, *48*, 1432−1440.
(25) Zuehlsdorff, T. J.; Isborn, C. M. Modeling absorption spectra of molecules in solution. *Int. J. Quantum Chem.* **2019**, *119*, e25719.
(26) Karbalaei Khani, S.; Marefat Khah, A.; Hättig, C. COSMO-RI-ADC(2) excitation energies and excited state gradients. *Phys. Chem. Chem. Phys.* **2018**, *20*, 16354−16363.
(27) Wenzel, J.; Wormit, M.; Dreuw, A. Calculating Core-Level Excitations and X-Ray Absorption Spectra of Medium-Sized Closed-Shell Molecules with the Algebraic-Diagrammatic Construction Scheme for the Polarization Propagator. *J. Comput. Chem.* **2014**, *35*, 1900−1915.
(28) Plasser, F.; Crespo-Otero, R.; Pederzoli, M.; Pittner, J.; Lischka, H.; Barbatti, M. Surface Hopping Dynamics with Correlated Single-Reference Methods: 9H-Adenine as a Case Study. *J. Chem. Theory Comput.* **2014**, *10*, 1395−1405.
(29) Klamt, A.; Schüürmann, G. COSMO: a new approach to dielectric screening in solvents with explicit expressions for the screening energy and its gradient. *J. Chem. Soc., Perkin Trans. 2* **1993**, *2*, 799−805.
(30) Peral, F.; Gallego, E. A study by ultraviolet spectroscopy on the self-association of diazines in aqueous solution. *Spectrochim. Acta, Part A* **2003**, *59*, 1223−1237.
(31) Linert, I.; Zubek, M. Electron energy-loss spectroscopy of excited states of the diazine molecules: Pyridazine. *J. Electron Spectrosc. Relat. Phenom.* **2019**, *233*, 69−76.
(32) Samir, B.; Kalalian, C.; Roth, E.; Salghi, R.; Chakir, A. Gas-phase UV absorption spectra of pyrazine, pyrimidine and pyridazine. *Chem. Phys. Lett.* **2020**, *751*, 137469.
(33) Marx, D.; Hutter, J. *Ab Initio Molecular Dynamics: Basic Theory and Advanced Methods*; Cambridge University Press: 2009.
(34) van der Spoel, D.; Lindahl, E.; Hess, B.; Groenhof, G.; Mark, A. E.; Berendsen, H. J. C. GROMACS: Fast, flexible, and free. *J. Comput. Chem.* **2005**, *26*, 1701−1718.
(35) Hess, B.; Kutzner, C.; van der Spoel, D.; Lindahl, E. GROMACS 4: Algorithms for Highly Efficient, Load-Balanced, and Scalable Molecular Simulation. *J. Chem. Theory Comput.* **2008**, *4*, 435−447.
(36) Pronk, S.; Páll, S.; Schulz, R.; Larsson, P.; Bjelkmar, P.; Apostolov, R.; Shirts, M. R.; Smith, J. C.; Kasson, P. M.; van der Spoel, D.; et al. GROMACS 4.5: a high-throughput and highly parallel open source molecular simulation toolkit. *Bioinformatics* **2013**, *29*, 845−854.
(37) Abraham, M. J.; van der Spoel, D.; Lindahl, E.; Hess, B. The G development team, GROMACS User Manual version 2019; available from http://www.gromacs.org.
(38) Sousa da Silva, A. W.; Vranken, W. F. ACPYPE - AnteChamber PYthon Parser interfacE. *BMC Res. Notes* **2012**, *5*, 367.
(39) Abascal, J. L. F.; Vega, C. A general purpose model for the condensed phases of water: TIP4P/2005. *J. Chem. Phys.* **2005**, *123*, 234505.
(40) Vega, C.; Abascal, J. L. F. Simulating water with rigid non-polarizable models: a general perspective. *Phys. Chem. Chem. Phys.* **2011**, *13*, 19663−19688.
(41) Parrinello, M.; Rahman, A. Polymorphic transitions in single crystals: A new molecular dynamics method. *J. Appl. Phys.* **1981**, *52*, 7182−7190.
(42) Bussi, G.; Donadio, D.; Parrinello, M. Canonical sampling through velocity rescaling. *J. Chem. Phys.* **2007**, *126*, 014101.
(43) Hutter, J.; Iannuzzi, M.; Schiffmann, F.; VandeVondele, J. CP2K: atomistic simulations of condensed matter systems. *WIREs Comput. Mol. Sci.* **2014**, *4*, 15−25.
(44) Kühne, T. D.; Iannuzzi, M.; Del, M.; Rybkin, V. V.; Seewald, P.; Stein, F.; Laino, T.; Khaliullin, R. Z.; Schütt, O.; Schiffmann, F.; et al. CP2K: An electronic structure and molecular dynamics software package - Quickstep: Efficient and accurate electronic structure calculations. *J. Chem. Phys.* **2020**, *152*, 194103.
(45) VandeVondele, J.; Krack, M.; Mohamed, F.; Parrinello, M.; Chassaing, T.; Hutter, J. QUICKSTEP: Fast and accurate density functional calculations using a mixed Gaussian and plane waves approach. *Comput. Phys. Commun.* **2005**, *167*, 103−128.
(46) Goedecker, S.; Teter, M.; Hutter, J. Separable dual-space Gaussian pseudopotentials. *Phys. Rev. B: Condens. Matter Mater. Phys.* **1996**, *54*, 1703−1710.
(47) Hartwigsen, C.; Goedecker, S.; Hutter, J. Relativistic separable dual-space Gaussian pseudopotentials from H to Rn. *Phys. Rev. B: Condens. Matter Mater. Phys.* **1998**, *58*, 3641−3662.
(48) Krack, M. Pseudopotentials for H to Kr optimized for gradient-corrected exchange-correlation functionals. *Theor. Chem. Acc.* **2005**, *114*, 145−152.
(49) Hammer, B.; Hansen, L. B.; Nørskov, J. K. Improved adsorption energetics within density-functional theory using revised Perdew-Burke-Ernzerhof functionals. *Phys. Rev. B: Condens. Matter Mater. Phys.* **1999**, *59*, 7413−7421.
(50) Grimme, S.; Antony, J.; Ehrlich, S.; Krieg, H. A consistent and accurate ab initio parametrization of density functional dispersion correction (DFT-D) for the 94 elements H-Pu. *J. Chem. Phys.* **2010**, *132*, 154104.

https://doi.org/10.1021/acs.jpca.1c05183
J. Phys. Chem. A 2021, 125, 7198−7206

(51) Forster-Tonigold, K.; Groß, A. Dispersion corrected RPBE studies of liquid water. *J. Chem. Phys.* **2014**, *141*, 064501.
(52) Martyna, G. J.; Klein, M. L.; Tuckerman, M. Nosé-Hoover chains: The canonical ensemble via continuous dynamics. *J. Chem. Phys.* **1992**, *97*, 2635−2643.
(53) Neese, F. Software update: the ORCA program system, version 4.0. *Wiley Interdiscip. Rev.: Comput. Mol. Sci.* **2018**, *8*, e1327.
(54) Neese, F.; Wennmohs, F.; Becker, U.; Riplinger, C. The ORCA quantum chemistry program package. *J. Chem. Phys.* **2020**, *152*, 224108.
(55) Ahlrichs, R.; Armbruster, M. K.; Bachorz, R. A.; Bahmann, H.; Baldes, A.; Bär, M.; Baron, H.-P.; Bauernschmitt, R.; Bischoff, F. A.; Böcker, S.; et al. TURBOMOLE V7.5 2020, a development of University of Karlsruhe and Forschungszentrum Karlsruhe GmbH, 1989−2007, TURBOMOLE GmbH, since 2007; available from https://www.turbomole.org.
(56) Balasubramani, S. G.; Chen, G. P.; Coriani, S.; Diedenhofen, M.; Frank, M. S.; Franzke, Y. J.; Furche, F.; Grotjahn, R.; Harding, M. E.; Hättig, C.; et al. TURBOMOLE: Modular program suite for ab initio quantum-chemical and condensed-matter simulations. *J. Chem. Phys.* **2020**, *152*, 184107.
(57) Schwabe, T.; Sneskov, K.; Haugaard Olsen, J. M.; Kongsted, J.; Christiansen, O.; Hättig, C. PERI-CC2: A Polarizable Embedded RI-CC2Method. *J. Chem. Theory Comput.* **2012**, *8*, 3274−3283.
(58) Corni, S.; Cammi, R.; Mennucci, B.; Tomasi, J. Electronic excitation energies of molecules in solution within continuum solvation models: Investigating the discrepancy between state-specific and linear-response methods. *J. Chem. Phys.* **2005**, *123*, 134512.
(59) Cederbaum, L. S.; Domcke, W.; Schirmer, J. Many-body theory of core holes. *Phys. Rev. A: At., Mol., Opt. Phys.* **1980**, *22*, 206−222.
(60) Costantini, R.; Faber, R.; Cossaro, A.; Floreano, L.; Verdini, A.; Hattig, C.; Morgante, A.; Coriani, S.; Dell'Angela, M. Picosecond timescale tracking of pentacene triplet excitons with chemical sensitivity. *Commun. Phys.* **2019**, *2*, 56.
(61) Hatsui, T.; Shigemasa, E.; Kosugi, N. Design of a Transmission Grating Spectrometer and an Undulator Beamline for Soft X-ray Emission Studies. *AIP Conf. Proc.* **2003**, *705*, 921−924.
(62) Nagasaka, M.; Yuzawa, H.; Kosugi, N. Soft X-ray Absorption Spectroscopy of Liquids for Understanding Chemical Processes in Solution. *Anal. Sci.* **2020**, *36*, 95−105.
(63) Nagasaka, M.; Kosugi, N. Soft X-ray Absorption Spectroscopy for Observing Element-specific Intermolecular Interaction in Solution Chemistry. *Chem. Lett.* **2021**, *50*, 956−964.
(64) Nagasaka, M.; Yuzawa, H.; Horigome, T.; Kosugi, N. Reliable Absorbance Measurement of Liquid Samples in Soft X-ray Absorption Spectroscopy in Transmission Mode. *J. Electron Spectrosc. Relat. Phenom.* **2018**, *224*, 93−99.
(65) Flesch, R.; Pavlychev, A. A.; Neville, J. J.; Blumberg, J.; Kuhlmann, M.; Tappe, W.; Senf, F.; Schwarzkopf, O.; Hitchcock, A. P.; Rühl, E. Dynamic Stabilization in $1\sigma_u \rightarrow 1\pi_g$ Excited Nitrogen Clusters. *Phys. Rev. Lett.* **2001**, *86*, 3767−3770.
(66) Luzanov, A. V.; Sukhorukov, A. A.; Umanskii, V. É. Application of transition density matrix for analysis of excited states. *Theor. Exp. Chem.* **1976**, *10*, 354−361.
(67) Luzanov, A. V.; Zhikol, O. A. Excited State Structural Analysis: TDDFT and Related Models. In *Practical Aspects of Computational Chemistry*; Leszczynski, J., Shukla, M. K., Eds.; Springer: Heidelberg, Germany, 2012; Vol. *I*, pp 415−449.
(68) Martin, R. L. Natural transition orbitals. *J. Chem. Phys.* **2003**, *118*, 4775−4777.
(69) Mayer, I. Using singular value decomposition for a compact presentation and improved interpretation of the CIS wave functions. *Chem. Phys. Lett.* **2007**, *437*, 284−286.

https://doi.org/10.1021/acs.jpca.1c05183
J. Phys. Chem. A 2021, 125, 7198−7206